Temporal and spatial variation of the drag coefficient of a developing sea under steady wind-forcing

Paul A. Hwang

Oceanography Division, Naval Research Laboratory, Stennis Space Center, Mississippi, USA

Received 7 February 2005; revised 18 April 2005; accepted 4 May 2005; published 29 July 2005.

[1] Field data indicate convincingly that the drag coefficient of the ocean surface is sea-state dependent. As a result, under steady forcing by a constant wind velocity the wind stress on the ocean surface varies with time. It also varies with space if the wave development is limited by fetch. A quantitative estimation of the temporal and spatial variation of the wind stress produced by a constant wind velocity is presented. The method of computation combines the duration- or fetch-limited growth functions of wind-generated waves and the similarity relation of the ocean-surface drag coefficient derived from wavelength scaling. The only required input is the wind speed. The results indicate that the average momentum flux from atmosphere to ocean is much larger (about 50 to 100 percent higher, and especially for shorter wind events) in comparison with calculations using the drag coefficient or dynamic roughness formulated either without the wave parameters or based on steady state wave conditions.

Citation: Hwang, P. A. (2005), Temporal and spatial variation of the drag coefficient of a developing sea under steady wind-forcing, *J. Geophys. Res.*, *110*, C07024, doi:10.1029/2005JC002912.

1. Introduction

[2] Over the last several decades, many wind stress measurements have been collected from oceans and lakes. These measurements are used to investigate the dependence of the drag coefficient and the dynamic roughness of the ocean surface on various environmental parameters. The reference wind speed by convention is U_{10}, the equivalent wind speed at 10-m elevation under the condition of neutral stratification. In the intermediate wind speed range (approximately from 7 to 20 m/s) under which the ocean surface is hydrodynamically rough, the corresponding drag coefficient, C_{10}, displays a general tendency of increasing with wind speed [e.g., *Garratt*, 1977; *Wu*, 1980]. Additional dependence on other sea-state parameters, especially the wave age, is also evident, but the data scatter is large and a quantitative determination of the additional sea-state dependence remains unsettled [e.g., *Donelan*, 1990; *Toba et al.*, 1990; *Geernaert*, 1999; *Jones and Toba*, 2001; *Drennan et al.*, 2003; *Smedman et al.*, 2003; *Guan and Xie*, 2004, and references therein]. Outside the intermediate wind speed range, different physics govern the behavior of the ocean-surface drag. For lower wind speeds, the ocean surface is either in hydrodynamically smooth or transitional regime and the wave influence is competing with the viscous effects [e.g., *Donelan*, 1990]. For very high wind speeds (say, above 25 m/s), extensive breaking occurs. The resulting spume, flying spray, and broad regions with flow separation act like a shroud shielding the fine-scale wave roughness from the airflow. Field measurements indicate that C_{10} reaches a maximum near 35 m/s and then decreases with increasing wind speeds [*Powell et al.*, 2003].

0148-0227/05/2005JC002912$09.00

[3] The following discussions focus on the surface wave effects without the complication of extensive wave breaking that leads to a reduced effective surface roughness, and limit the scope of investigation to locally generated waves by steady winds of intermediate velocities and neutral stratification. From the wave dynamics point of view, the more meaningful reference elevation should be the characteristic wavelength, λ_p [e.g., *Kitaigorodskii*, 1973; *Stewart*, 1974; *Donelan*, 1990; *Makin and Kudryavtsev*, 2002; *Oost et al.*, 2002; *Hwang*, 2004], because the influence of surface waves decays exponentially with the distance from the air-sea interface and the wavelength serves as the length scale of the attenuation rate [e.g., *Miles*, 1957; *Phillips*, 1977]. *Oost et al.* [2002] presented data showing an excellent correlation between the wind friction velocity, u_*, and the wind speed at an elevation proportional to the wavelength, $U_{\lambda/2}$ or U_λ, for measurements under neutral stratification and wind-sea dominant conditions; the correlation coefficient reaches 0.964. *Hwang* [2004] carried out an analysis of the drag coefficient $C_{\lambda/2}$ referenced to $U_{\lambda/2}$. The wavelength scaling yields considerable improvement in collapsing field measurements of the drag coefficient. The assembled data set, to be further discussed in section 2, covers a wide range of the sea-state conditions: $0.0235 < \omega_p u_*/g < 0.237$, $0.0263 < u_*/c_p < 0.237$, where ω_p and c_p are, respectively, the angular frequency and the phase velocity of the wave component at the spectral peak, and g is the gravitational acceleration. The correlation coefficient, Q_c, and the relative root mean square (RMS) difference, S, between the fitted function $C_{\lambda/2}(\omega_p u_*/g)$ and measured data are 0.949 and 0.017, respectively. In comparison, the range of (Q_c, S) for various C_{10} functions is (0.55–0.79, 0.025–0.034) [*Hwang*, 2005a]. These results strongly suggest that the similarity relation of the ocean-

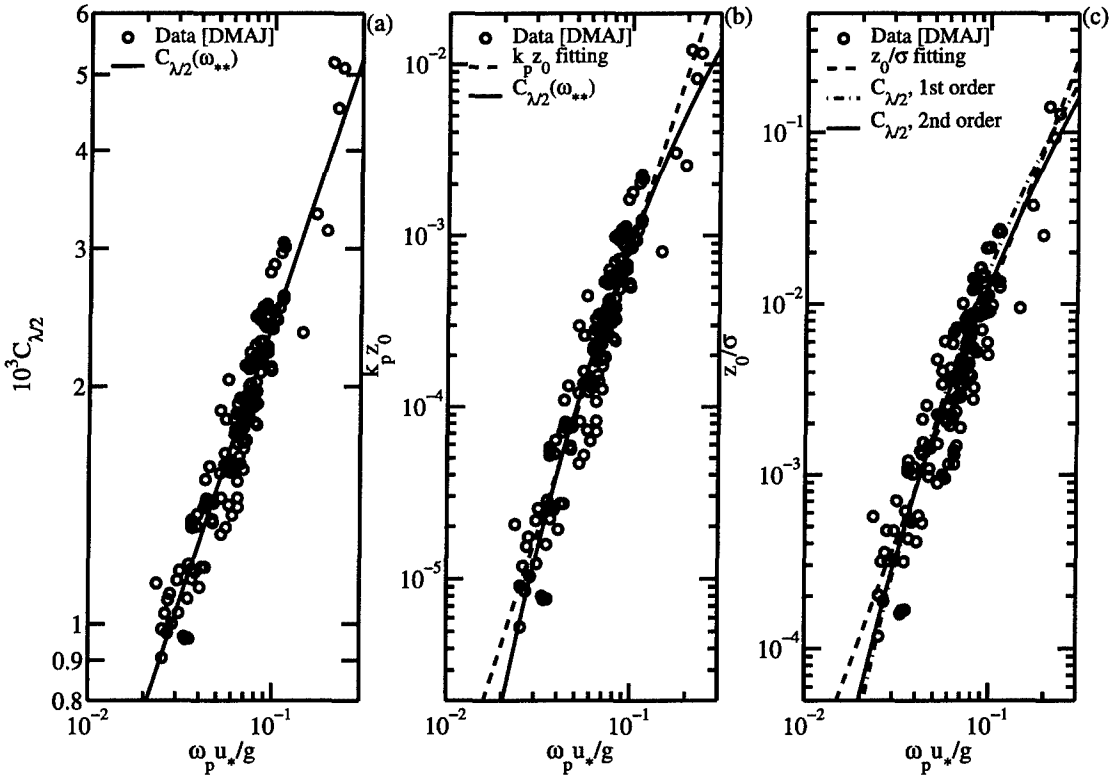

Figure 1. (a) Drag coefficient $C_{\lambda/2}(\omega_p u_*/g)$ measured in wind-sea dominant conditions (DMAJ data set), and dimensionless roughness (b) $k_p z_0(\omega_p u_*/g)$ and (c) $z_0/\sigma(\omega_p u_*/g)$.

surface drag coefficient exists in wavelength scaling. For practical applications, it is necessary to convert the similarity relation of $C_{\lambda/2}$ to C_{10}, which is not a trivial problem.

[4] In this paper, a few solutions are presented to quantify the dependence of C_{10} on wind speed and sea state based on the similarity relation of $C_{\lambda/2}$ (section 2). Because the development of wind-generated waves is duration- and fetch-dependent, it follows that the drag coefficient of the ocean surface under steady forcing by a constant wind velocity is temporally and spatially varying. The air-sea momentum flux computed with the drag coefficient or dynamic roughness established under steady state wave conditions or without considering the wave factor would underestimate the actual magnitude of the wind input into the water body. Combining the similarity relation of the drag coefficient derived from wavelength scaling and the growth functions of wind-generated waves, the calculated C_{10} displays significant temporal and spatial variations. Its magnitude is about a factor of 2 higher in the first couple of hours or kilometers compared to the values at the mature-wave stage (section 3). Additional discussions on the correlation between the drag coefficient and the dynamic roughness are presented in section 4, and a summary is given in section 5.

2. Drag Coefficient of the Ocean Surface

2.1. Wavelength Scaling

[5] With the wavelength scaling, the drag coefficient is represented by $C_{\lambda/2} = u_*^2/U_{\lambda/2}^2$. Applying this scaling to field data measured under the condition of local wind-wave generation [*Donelan*, 1979; *Merzi and Graf*, 1985; *Anctil and Donelan*, 1996; *Janssen*, 1997] (hereinafter referred to as the DMAJ data set; the experimental conditions were summarized by *Hwang* [2004]), the data scatter of $C_{\lambda/2}$ given as a function of $\omega_p u_*/g$ is markedly reduced in comparison to that of C_{10} functions. The following function, shown as the solid curve in Figure 1a, is established from the DMAJ data set,

$$C_{\lambda/2} = A_c\left(\frac{\omega_p u_*}{g}\right)^{a_c}, \tag{1}$$

with $A_c = 1.220 \times 10^{-2}$, $a_c = 0.704$, and $(Q_c, S) = (0.949, 0.017)$.

[6] With wavelength scaling, $k_p z_0$ is the natural expression of the dimensionless roughness, where k_p is the wave number at the spectral peak. Applying the function of logarithmic wind speed profile to equation (1), the dimensionless roughness is given by

$$k_p z_0 = \pi \exp\left(-\kappa C_{\lambda/2}^{-0.5}\right), \tag{2}$$

where $\kappa = 0.4$ is the von Kármán constant. Equation (2) is shown as the solid curve in Figure 1b. For comparison, the dashed curve is the data-fitting function $k_p z_0 = 1.889(\omega_p u_*/g)^{3.327}$, with $(Q_c, S) = (0.949, 0.062)$.

[7] Figure 1c displays the result of normalizing z_0 with the RMS surface displacement, σ. The dimensionless roughness expressed as the Charnock parameter, $z_{0_*} = z_0 g/u_*^2$, is more scattered, with $(Q_c, S) = (0.802, 0.159)$. Because $z_0/\sigma = k_p z_0/s_*^{0.5}$, where $s_* = k_p^2\sigma^2$, which is equivalent to $e_*\omega_*^4$ for deep-water waves, $e_* = \sigma^2 g^2/U_{10}^4$, and $\omega_* = \omega_p U_{10}/g$,

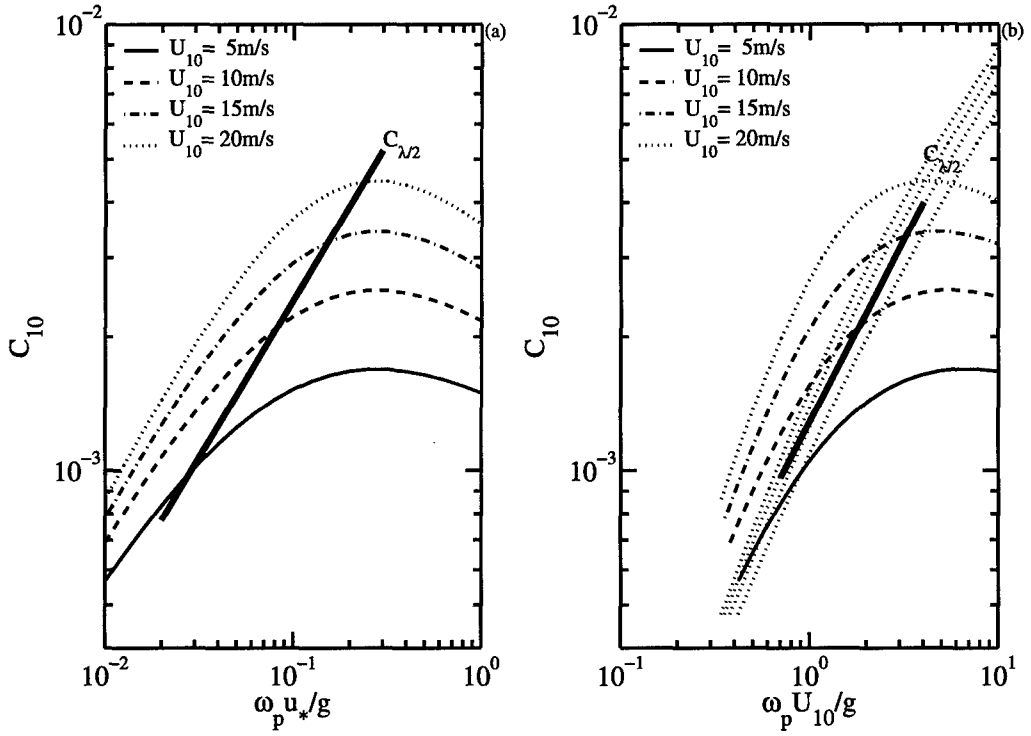

Figure 2. C_{10} computed from equation (1), plotted as a function of (a) $\omega_p u_*/g$ and (b) $\omega_p U_{10}/g$. See text for the description of the $C_{\lambda/2}$ curves.

fetch-growth functions can be used to correlate $k_p z_0$ and z_0/σ. *Hwang and Wang* [2004, 2005] developed a higher-order data-fitting technique to obtain the empirical power law wave-growth functions with variable wave development rates; that is, the exponents of the power law functions may vary with the dimensionless fetch, duration, or wave frequency. For the present illustration, the growth function is represented by the dependence of the dimensionless wave energy on the dimensionless wave frequency,

$$e_* = R\omega_*^r. \tag{3}$$

For the first-order-fitted function, $R_1 = 2.94 \times 10^{-3}$, $r_1 = -3.42$, and for the second-order-fitted function, $R_2 = \exp(-6.1384)\omega_*^{0.6102\ln\omega_*}$, $r_2 = -2.4019 - 1.2204\ln\omega_*$ [*Hwang*, 2005b]. The results of converting $k_p z_0$ to z_0/σ using the wave-growth functions are shown in Figure 1c. For comparison, the data-fitting function $z_0/\sigma = 8.345(\omega_p u_*/g)^{2.863}$, with $(Q_c, S) = (0.927, 0.099)$, is also shown. The results illustrated in Figure 1 suggest that the similarity relation of the ocean-surface drag coefficient exists in wavelength scaling, and that equation (1) can be used to represent both the drag coefficient and the dynamic roughness of the ocean surface.

2.2. Conversion to 10-m Reference Elevation

[8] For practical applications, the height of reference wind speed is generally set at 10 m. The drag coefficients C_{10} and $C_{\lambda/2}$ are related by

$$C_{10} = C_{\lambda/2} R_U^2, \tag{4a}$$

$$C_{10} = \left[\frac{1}{\kappa}\ln\left(\frac{k_p 10}{k_p z_0}\right)\right]^{-2}, \tag{4b}$$

$$R_U = \frac{U_{\lambda/2}}{U_{10}} = \frac{\ln\pi - \ln(k_p z_0)}{\ln\left(\dfrac{\omega_{**}^2 g 10}{C_{\lambda/2} k_p z_0 U_{10}^2}\right) - 2\ln(R_U)}, \tag{5}$$

and $\omega_{**} = \omega_p u_*/g$. It is of interest to investigate the properties of C_{10} as a function of wind speed and sea-state parameters based on the similarity function of $C_{\lambda/2}$ described in the last section. If ω_{**} and k_p are given, the procedure to derive C_{10} is applying equation (1) to obtain $C_{\lambda/2}(\omega_{**})$, then equation (2) to obtain $k_p z_0(\omega_{**})$, and finally equation (4b) to derive $C_{10}(\omega_{**}, k_p)$. Of more interest is $C_{10}(\omega_{**}, U_{10})$, which can be derived by equations (1), (2), (5), and (4a). R_U can be solved iteratively for given ω_{**} and U_{10}. From numerical experiment, with the initial guess of $R_{U0} = 1$, a relative error of 1% is achieved within five iterations. Figure 2a displays the computed $C_{10}(\omega_p u_*/g)$ for a range of ω_{**} and U_{10}. For comparison, the $C_{\lambda/2}(\omega_p u_*/g)$ curve (equation (1)) is also graphed in the same panel with a thick line segment. While $C_{\lambda/2}$ increases monotonically with $\omega_p u_*/g$, C_{10} curves show local maximum near $\omega_p u_*/g = 0.25$. The points where C_{10} curves intercept the $C_{\lambda/2}$ curve correspond to the condition that the peak wavelength is 20 m and $C_{10} = C_{\lambda/2}$. Toward the right-hand side (younger waves) of the interceptions, C_{10} represents the drag coefficient referenced to a wind speed higher than $U_{\lambda/2}$, resulting in a lower magnitude. Similarly, toward the left-hand side of the interceptions, $U_{10} < U_{\lambda/2}$ therefore $C_{10} > C_{\lambda/2}$.

[9] Both $C_{\lambda/2}(\omega_p u_*/g)$ and $C_{10}(\omega_p u_*/g)$ can be given in terms of $\omega_p U_{10}/g$ by the substitution of

$$\frac{\omega_p U_{10}}{g} = \frac{\omega_p u_*/g}{R_U C_{\lambda/2}^{0.5}}. \tag{6}$$

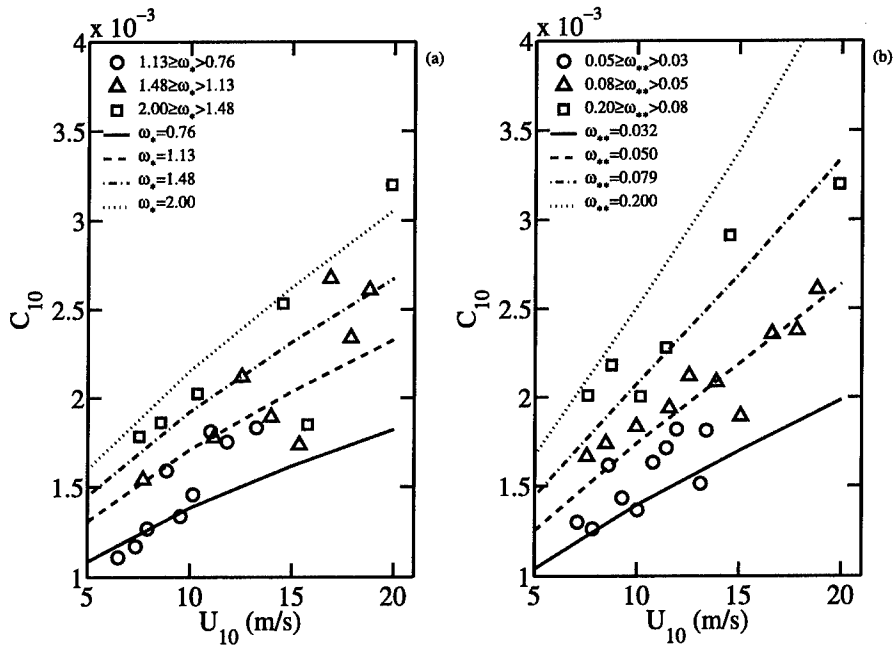

Figure 3. (a) C_{10} calculated using equation (7) and presented as a function of U_{10}; (b) same as Figure 3a, but C_{10} is calculated using equation (1). The DMAJ data are superimposed for comparison.

The resulting $C_{10}(\omega_p U_{10}/g)$ curves for U_{10} = 5, 10, 15, and 20 m/s are shown in Figure 2b. Also superimposed in this figure are the corresponding $C_{\lambda/2}(\omega_p U_{10}/g)$ curves, shown as dotted lines that increase monotonically with $\omega_p U_{10}/g$. The thick line segment plotted in Figure 2b is the empirical function derived from data fitting of the DMAJ data set

$$C_{\lambda/2} = A_{10}\left(\frac{\omega_p U_{10}}{g}\right)^{a_{10}}, \tag{7}$$

with $A_{10} = 1.289 \times 10^{-3}$, $a_{10} = 0.815$, and $(Q_c, S) = (0.893, 0.024)$ [*Hwang*, 2005a].

[10] From the point-of-view of practical applications, equation (7) is more convenient than equation (1) for obtaining C_{10} using the similarity relation of the drag coefficient derived from wavelength scaling. If ω_* and k_p are given, the procedure to obtain $C_{10}(\omega_*, k_p)$ is straightforward, through equations (7), then (2) and (4b). To derive $C_{10}(\omega_*, U_{10})$, only a slight modification of the procedure is needed: k_p can be calculated from the dispersion relation because $\omega_p (= \omega_* g/U_{10})$ is available. Also, $C_{10}(\omega_*, U_{10})$ can be constructed from equation (7) with ω_p and U_{10} input. For intermediate- and shallow-water wave conditions, the additional information of water depth is needed to obtain k_p from ω_p to apply equation (4b). Numerical computations show that equations (1) and (7) produce very similar C_{10} at about 10 m/s wind speed. At higher wind speeds, equation (7) yields lower C_{10} compared to equation (1), and vise versa at lower wind speeds. The difference is generally within 25% of each other. Figure 3a shows C_{10} curves computed with equations (7), (2), and (4b). Superimposed on these curves are the DMAJ data sorted into three ω_* bins and ensemble-averaged over 10 wind speed sub-ranges for each ω_* bin to match the computational curves. For comparison, the results computed using equations (1), (2), (5), and (4a) are displayed in Figure 3b with DMAJ data superimposed.

[11] In the literature, C_{10} is frequently expressed as a linear function of U_{10}. The slope of the linear function is generally steeper for younger seas and milder for more mature seas [e.g., *Guan and Xie*, 2004], a feature that is consistent with the result shown in Figure 3. It should be pointed out that representing C_{10} as a linear function of U_{10} is dimensionally inconsistent, and it yields a constant wind stress for a constant wind speed. Although the sea-state influence can be included through introducing sea-state dependence for the slope of the linear function, it remains unsatisfactory that such an expression is dimensionally inconsistent.

3. Temporal and Spatial Variation of the Drag Coefficient

[12] Because wave development is dependent on fetch and duration, under steady wind forcing the wind stress exerted on the water surface varies with time and space as a consequence of the sea-state dependence of the drag coefficient. The spatial and temporal variation of the wind stress can be quantified through the fetch- and duration-limited wave-growth functions

$$e_* = \begin{cases} Ax_*^a \\ Pt_*^p \end{cases}$$
$$\omega_* = \begin{cases} Bx_*^b \\ Qt_*^q \end{cases}, \tag{8}$$

where $x_* = xg/U_{10}^2$, x is fetch, $t_* = tg/U_{10}$, and t is duration. The coefficients of the duration-limited growth functions

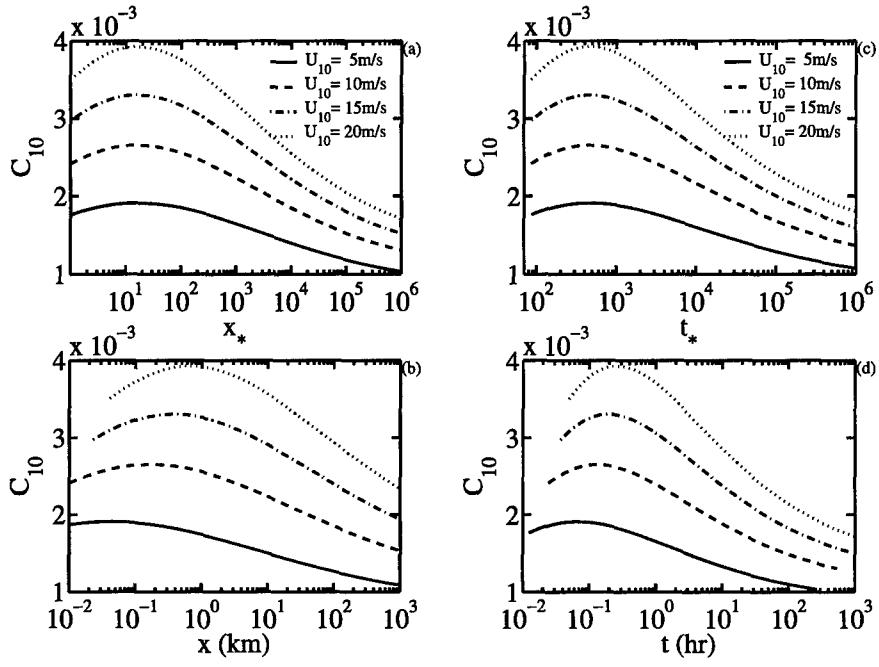

Figure 4. Spatial and temporal variation of C_{10} under steady wind forcing in (a, c) dimensionless fetch and duration, respectively, and (b, d) in dimensional fetch and duration, respectively.

can be written in terms of the coefficients of the fetch-limited growth functions [*Hwang and Wang*, 2004, 2005],

$$P = A\left[\frac{R_c(b+1)}{B}\right]^{\frac{a}{b+1}} \quad p = \frac{a}{b+1}$$
$$Q = \left[B^{\frac{1}{b}}R_c(b+1)\right]^{\frac{b}{b+1}} \quad q = \frac{b}{b+1}, \tag{9}$$

where R_c is the ratio between the effective group and phase velocities of the wave component at the spectral peak. For wind seas, $R_c \approx 0.4$ [*Yefimov and Babanin*, 1991]. Generally, the fetch- and duration-limited wave growth data can be represented by first-order-fitted power law functions (with constant exponents) [*Hwang and Wang*, 2004, 2005] for the fetch range $\sim 10^2 < x_* < \sim 10^4$. The coefficients are $A_1 = 6.19 \times 10^{-7}$, $a_1 = 0.811$, $B_1 = 11.86$, $b_1 = -0.237$, $P_1 = 1.27 \times 10^{-8}$, $p_1 = 1.062$, $Q_1 = 36.92$, and $q_1 = -0.310$. For a broader coverage of x_* the development rate is not constant. The variable development rate can be obtained from data by using a higher-order polynomial function in log-log scales for data fitting. To the second order, the coefficients of the fetch laws become

$$A_2 = e^{\alpha_0} x_*^{-\alpha_2 \ln x_*} \quad a_2 = \alpha_1 + 2\alpha_2 \ln x_*$$
$$B_2 = e^{\beta_0} x_*^{-\beta_2 \ln x_*} \quad b_2 = \beta_1 + 2\beta_2 \ln x_*, \tag{10}$$

with $\alpha_0 = 3.0377$, $\alpha_1 = -0.3990$, $\alpha_2 = 0.0110$, $\beta_0 = -17.6158$, $\beta_1 = 1.7645$, and $\beta_2 = -0.0647$. The corresponding coefficients of the second-order-fitted power law functions for $e_*(t_*)$ and $\omega_*(t_*)$ can be calculated by equations (10) and (9). Applying the above wave-growth functions to derive the dimensionless frequency, the spatial and temporal evolution of C_{10} under steady wind forcing can be calculated with equations (7), (2), and (4b). Figure 4 shows C_{10} as a function of dimensionless or dimensional fetch and duration for wind speeds between 5 and 20 m/s. A much larger drag coefficient at the early stage of wave development is evident. The average wind stress in the first 2 hours of a wind event is about 50 to 70% higher than that at the mature-sea stage.

4. Discussion

[13] There has been considerable uncertainty about the quantitative properties of the drag coefficient of the ocean surface. It was initially considered to be a constant and later revised to be increasing with wind speed. Although it remains unsettled on how the drag coefficient increases with wind speed, field data suggest that the rate of increase is sea-state dependent. Another approach to studying the sea-surface drag is through the investigation of the dynamic roughness. (This seems to be a unique feature of the ocean-surface drag; almost all other branches of fluid mechanics describe the surface drag by the drag coefficient, expressed correctly in dimensionally consistent functions.) The Charnock parameter, $z_{0*} = z_0 g/u_*^2$, was originally considered to be a constant [*Charnock*, 1955], but later was also found to be sea-state dependent. *Donelan* [1990] normalized z_0 by σ. The resulting function is much more successful in explaining measurements from disparate experiments. While there is good progress in characterizing z_0, it remains a puzzle that the behavior of its counterpart, the drag coefficient, is so difficult to understand. The dynamic roughness z_0 is not a measured quantity. Its derivation depends on the application of the logarithmic wind profile, which can be written as

$$C_z^{-0.5} = \frac{1}{\kappa} \ln \frac{z}{z_0}, \tag{11}$$

where C_z is the drag coefficient referenced to the wind speed at elevation z. The correlation of the drag coefficient and the dynamic roughness should be one-to-one and deterministic as elicited by equation (11).

[14] *Hwang* [2004] suggested that the difficulty in finding the similarity properties of the ocean-surface drag coefficient can be attributed to the choice of the arbitrary 10 m as the length scale for wind speed reference. Indeed, when processed with wavelength scaling, the wind stress measurements in oceans or lakes under wind-sea dominant conditions, either represented by the drag coefficient or by the dynamic roughness, show strong similarity behavior on $\omega_p u_*/g$ (Figure 1).

5. Summary

[15] The drag coefficient is sea-state dependent, so although the forcing wind velocity is constant and steady, the wind stress on the ocean surface varies with time and space. The temporal and spatial variation of the wind stress represented by C_{10} is quantified by combining the similarity relation of the drag coefficient and the growth functions of wind-generated waves. The results show that the wind stress is much larger in the first few hours of a wind event than that at a later time when the wave field is more mature. Wind stress computations using the drag coefficient or dynamic roughness formulated without considering the wave factors or based on steady state wave conditions may underestimate the wind input into the ocean by as much as a factor of 2 (Figure 4). The procedure described in this paper provides a parametric means to estimating the wave influence on the momentum transfer in a coupled air-sea interaction system in the absence of a numerical ocean wave model. It is relatively easy to use and requires only the wind speed input. The sea-state information is embedded in time and space through the wave-growth functions. The procedure outlined in this paper is applicable to wind-generated wave conditions in the field environment. The drag coefficient and dynamic roughness under mixed-sea conditions remain difficult to parameterize at this stage.

[16] **Acknowledgments.** This work is sponsored by the Office of Naval Research (Naval Research Laboratory PE61153N). Comments and suggestions from two anonymous reviewers are very helpful in improving the presentation of this paper. NRL contribution NRL/JA7330-04-5081.

References

Anctil, F., and M. A. Donelan (1996), Air-water momentum flux observed over shoaling waves, *J. Phys. Oceanogr.*, *26*, 1344–1353.

Charnock, H. (1955), Wind stress on a water surface, *Q. J. R. Meteorol. Soc.*, *81*, 639.

Donelan, M. A. (1979), On the fraction of wind momentum retained by waves, *Marine Forecasting*, edited by J. C. J. Nihoul, pp. 141–159, Elsevier, New York.

Donelan, M. A. (1990), Air-sea interaction, in *The Sea*, vol. 9, *Ocean Engineering Science*, edited by B. LeMehaute and D. M. Hanes, pp. 239–292, Wiley Intersci., Hoboken, N. J.

Drennan, W. M., H. C. Graber, D. Hauser, and C. Quentin (2003), On the wave age dependence of wind stress over pure wind seas, *J. Geophys. Res.*, *108*(C3), 8062, doi:10.1029/2000JC000715.

Garratt, J. R. (1977), Review of drag coefficients over oceans and continents, *Mon. Weather Rev.*, *105*, 915–929.

Geernaert, G. L. (Ed.) (1999), *Air-Sea Exchange: Physics, Chemistry and Dynamics*, 578 pp., Springer, New York.

Guan, C., and L. Xie (2004), On the linear parameterization of drag coefficient over sea surface, *J. Phys. Oceanogr.*, *34*, 2847–2851.

Hwang, P. A. (2004), Influence of wavelength on the parameterization of drag coefficient and surface roughness, *J. Oceanogr.*, *60*, 835–841.

Hwang, P. A. (2005a), Comparison of the ocean surface wind stress computed with different parameterization functions of the drag coefficient, *J. Oceanogr.*, *61*, 91–107.

Hwang, P. A. (2005b), Drag coefficient, dynamic roughness and reference wind speed, *J. Oceanogr.*, *61*, 399–413.

Hwang, P. A., and D. W. Wang (2004), Field measurements of duration-limited growth of wind-generated ocean surface waves at young stage of development, *J. Phys. Oceanogr.*, *34*, 2316–2326, Corrigendum, 35, 2005.

Hwang, P. A., and D. W. Wang (2005), Corrigendum: Field measurements of duration-limited growth of wind-generated ocean surface waves at young stage of development, *J. Phys. Oceanogr.*, *35*, 268.

Janssen, J. A. M. (1997), Does wind stress depend on sea-state or not?—A statistical error analysis of HEXMAX data, *Boundary Layer Meteorol.*, *83*, 479–503.

Jones, I. S. F., and Y. Toba (Eds.) (2001), *Wind Stress Over the Ocean*, 307 pp, Cambridge Univ. Press, New York.

Kitaigorodskii, S. A. (1973), *The Physics of Air-Sea Interaction* (Engl. Transl.), 237 pp., Isr. Program for Sci. Transl., Jerusalem.

Makin, V. K., and V. N. Kudryavtsev (2002), Impact of dominant waves on sea drag, *Boundary Layer Meteorol.*, *103*, 83–99.

Merzi, N., and W. H. Graf (1985), Evaluation of the drag coefficient considering the effects of mobility of the roughness elements, *Ann. Geophys.*, *3*, 473–478.

Miles, J. W. (1957), On the generation of surface waves by shear flow, *J. Fluid Mech.*, *3*, 185–204.

Oost, W. A., G. J. Komen, C. M. J. Jacobs, and C. Van Oort (2002), New evidence for a relation between wind stress and wave age from measurements during ASGAMAGE, *Boundary Layer Meteorol.*, *103*, 409–438.

Phillips, O. M. (1977), *The Dynamics of the Upper Ocean*, 336 pp., Cambridge Univ. Press, New York.

Powell, M. D., P. J. Vickery, and T. A. Reinhold (2003), Reduced drag coefficient for high wind speeds in tropical cyclones, *Nature*, *422*, 279–283.

Smedman, A., X. G. Larsén, U. Högström, K. K. Kahma, and H. Pettersson (2003), Effect of sea state on the momentum exchange over the sea during neutral conditions, *J. Geophys. Res.*, *108*(C11), 3367, doi:10.1029/2002JC001562.

Stewart, R. W. (1974), The air-sea momentum exchange, *Boundary Layer Meteorol.*, *6*, 151–167.

Toba, Y., N. Iida, H. Kawamura, N. Ebuchi, and I. S. F. Jones (1990), Wave dependence of sea-surface wind stress, *J. Phys. Oceanogr.*, *20*, 705–721.

Wu, J. (1980), Wind-stress coefficients over sea surface near neutral conditions —A revisit, *J. Phys. Oceanogr.*, *10*, 727–740.

Yefimov, V. V., and A. V. Babanin (1991), Dispersion relation for the envelope of groups of wind waves, *Izv. Atmos. Oceanic Phys.*, *27*, 599–603.

P. A. Hwang, Oceanography Division, Naval Research Laboratory, Stennis Space Center, MS 39529-5004, USA. (paul.hwang@nrlssc.navy.mil)

REPORT DOCUMENTATION PAGE

Form Approved
OMB No. 0704-0188

1. REPORT DATE *(DD-MM-YYYY)*	2. REPORT TYPE	3. DATES COVERED *(From - To)*
07-06-2006	Journal Article (refereed)	

4. TITLE AND SUBTITLE
Temporal and Spatial Variation of the Drag Coefficient of a Developing Sea Under Steady Wind-Forcing

5a. CONTRACT NUMBER

5b. GRANT NUMBER

5c. PROGRAM ELEMENT NUMBER
PE0601153N

6. AUTHOR(S)
Paul A. Hwang

5d. PROJECT NUMBER

5e. TASK NUMBER

5f. WORK UNIT NUMBER
73-8190-05

7. PERFORMING ORGANIZATION NAME(S) AND ADDRESS(ES)
Naval Research Laboratory
Oceanography Division
Stennis Space Center, MS 39529-5004

8. PERFORMING ORGANIZATION REPORT NUMBER
NRL/JA/7330-04-5081

9. SPONSORING/MONITORING AGENCY NAME(S) AND ADDRESS(ES)
Office of Naval Research
800 N. Quincy St.
Arlington, VA 22217-5660

10. SPONSOR/MONITOR'S ACRONYM(S)
ONR

11. SPONSOR/MONITOR'S REPORT NUMBER(S)

12. DISTRIBUTION/AVAILABILITY STATEMENT
Approved for public release, distribution is unlimited.

13. SUPPLEMENTARY NOTES

14. ABSTRACT
Field data indicate convincingly that the drag coefficient of the ocean surface is sea-state dependent. As a result, under steady forcing by a constant wind velocity the wind stress on the ocean surface varies with time. It also varies with space if the wave development is limited by fetch. A quantitative estimation of the temporal and spatial variation of the wind stress produced by a constant wind velocity is presented. The method of computation combines the duration- or fetch-limited growth functions of wind-generated waves and the similarity relation of the ocean-surface drag coefficient derived from wavelength scaling. The only required input is the wind speed. The results indicate that the average momentum flux from atmosphere to ocean is much larger (about 50 to 100 percent higher, and especially for shorter wind events) in comparison with calculations using the drag coefficient or dynamic roughness formulated either without the wave parameters or based on steady state wave conditions.

15. SUBJECT TERMS
Drag coefficient; Wavelength scaling; Charnock parameter;

16. SECURITY CLASSIFICATION OF:			17. LIMITATION OF ABSTRACT	18. NUMBER OF PAGES	19a. NAME OF RESPONSIBLE PERSON
a. REPORT	b. ABSTRACT	c. THIS PAGE			Paul A. Hwang
Unclassified	Unclassified	Unclassified	UL	6	19b. TELEPHONE NUMBER *(Include area code)* 301-412-4914